Cellular and Molecular Neurobiology (2025) 45:1
https://doi.org/10.1007/s10571-024-01507-z

ORIGINAL RESEARCH

TMEM16A Activation Inhibits Autophagy in Dorsal Root Ganglion Cells, Which is Associated with the p38 MAPK/mTOR Pathway

Shuyun Yang[1,2] · Hui Shang[1,2] · Yuruo Zhang[2] · Jingsong Qiu[3] · Zheyi Guo[1] · Yong Ma[1] · Yuhang Lan[1,2] · Shaoyang Cui[4] · Hongshuang Tong[1] · Guocai Li[1]

Received: 28 January 2024 / Accepted: 16 October 2024

Abstract

Transmembrane member 16A (TMEM16A) exhibits a negative correlation with autophagy, though the underlying mechanism remains elusive. This study investigates the mechanism between TMEM16A and autophagy by inducing autophagy in DRG neuronal cells using Rapamycin. Results indicated that TMEM16A interference augmented cell viability and reduced Rapamycin-induced apoptosis. Autophagosome formation increased with TMEM16A interference but decreased upon overexpression. A similar increase in autophagosomes was observed with SB203580 treatment. Furthermore, TMEM16A interference suppressed Rapamycin-induced gene and protein expression of p38 MAPK and mTOR, whereas overexpression had the opposite effect. These findings suggest that TMEM16A activation inhibits autophagy in DRG cells, which is associated with the p38 MAPK/mTOR pathway, offering a potential target for mitigating neuropathic pain (NP).

Graphical abstract

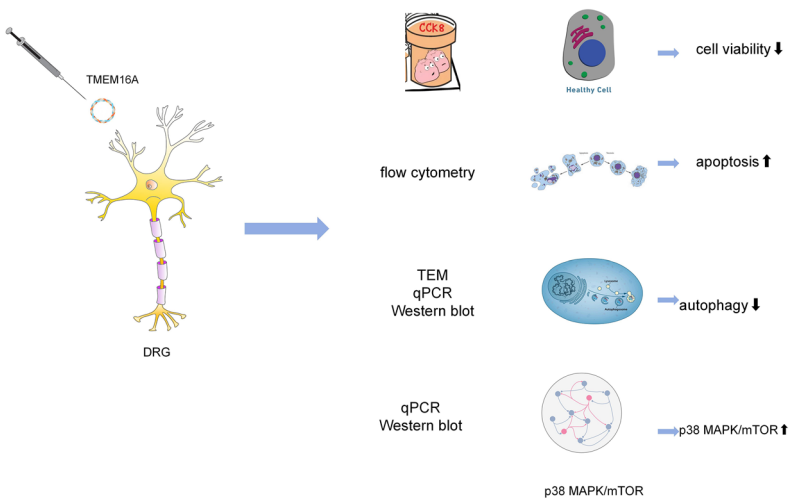

Keywords TMEM16A · Dorsal root ganglia · P38 MAPK · mTOR · Autophagy · Neuropathic pain

Introduction

Autophagy, a lysosome-mediated degradation pathway, plays a crucial role in maintaining intracellular environmental stability by degrading damaged and redundant organelle components such as amino acids, fatty acids, nucleosides, and other small molecules for cellular reuse (Ray 2020; Zhang

Shuyun Yang and Hui Shang contributed equally to this work and share first authorship.

Extended author information available on the last page of the article

Published online: 04 December 2024

et al. 2020; Debnath and Leidal 2022). Apoptosis is recognized and accepted as a unique and important "programmed" mode of cell death, which involves gene determined cell elimination. Apoptosis typically occurs during development and aging, and serves as a homeostatic mechanism for maintaining cell populations in tissues. The mechanism of cell apoptosis is very complex and involves an energy dependent cascade of molecular events. So far, research has shown that there are two main pathways of apoptosis: exogenous or death receptor pathways and intrinsic or mitochondrial pathways.

Transmembrane member 16A (TMEM16A), a member of the Tmem16 family of multiple transmembrane proteins, forms the molecular basis of calcium activated chloride channels (CaCCs) and is a thermosensitive protein in nociceptors (Chen et al. 2019; Lv et al. 2020). TMEM16A is expressed in nerve cells such as the dorsal root ganglian (DRG), neurons, and spinal cord neurons, which suggests that this channel is associated with some special sensory pathways. TMEM16A-CaCC produces a chloride current of ions, which mediates bradykinin to cause acute pain. TMEM16A-CaCC is also associated with membrane repolarization by producing electrical signals which regulate the particles en-tering and leaving the cell, thereby affecting the potential of the cell membrane and participating in nerve transmission. This property may potentially be exploited for blocking the nerve signals of pain (Zhong et al. 2021). Recent preliminary experimental results suggest a potential relationship between TMEM16A and autophagy, yet its specific mechanism remains unclear.

The mitogen-activated protein kinases (MAPKs) cascade pathway, an essential intracellular signal transduction pathway, includes p38 MAPK, a significant branch involved in various physiological processes (Qin et al. 2023; Gu et al. 2018). P38MAPK is instrumental in neuronal plasticity, pain signaling, and glial cell activation (Joo et al. 2018; Cai et al. 2022). Recent studies have identified p38MAPK as a convergence point of multiple signaling pathways, playing a role in autophagy regulation (Xu et al. 2023; Liao et al. 2020; He et al. 2021). The mammalian target of Rapamycin (mTOR), a relatively conserved serine/threonine protein kinase, is a central component of the autophagy signaling network and negatively regulates autophagy (Wang et al. 2018c; Paul et al. 2023; Ali et al. 2023). Research has established that p38MAPK activation can lead to increased mTOR expression, thereby activating the p38MAPK/mTOR pathway and subsequently inhibiting autophagy (Hou et al. 2023; Acharya et al. 2021; Yang et al. 2021).

Neuropathic pain (NP) is a condition resulting from injuries and diseases leading to dysfunctions in the sensory nervous system, characterized by altered function of the nervous system promoting phenomena like spontaneous pain, hyperalgesia, and allodynia. Epidemiological studies have shown that their prevalence in the general population may be as high as 7–8%, accounting for 20–25% of individuals with chronic pain (Torrance et al. 2006; Bouhassira et al. 2008). It represents a challenging chronic disease in clinical settings (Estivill-Torrús et al. 2024). Although autophagy is known to mediate the onset and progression of NP, the underlying mechanisms remain elusive. In our prior studies, we observed that the TMEM16A plasmid significantly inhibited Rapamycin (Rap)—induced autophagy in spinal DRG neurons, concomitantly with a notable upregulation of p38 and mTOR expression. This suggests TMEM16A's role in inhibiting DRG autophagy, but its association with the p38MAPK/mTOR pathway is yet to be determined. Therefore, our study focused on whether TMEM16A inhibition of DRG autophagy is associated with the p38 MAPK/mTOR pathway through in vitro experiments.

Experimental Materials and Methods (All materials tables are found in Appendix 1 of the supplement)

Cell Culture and Treatment

In our cell experiments, randomization and blinding were employed to ensure unbiased and reliable results. Cells were randomly assigned to different experimental and control groups using a random number generator. Treatments were administered in a random order to avoid temporal or environmental biases. Data collection was performed by personnel blinded to group assignments, ensuring that observations were not influenced by prior knowledge of the experimental conditions. Each condition was independently replicated at least three times to confirm the reproducibility and robustness of the results.

The thawed primary rat DRG cells (CP-R126, Procell) were moved from liquid nitrogen to a dry thermostatic heater using a dry ice container. Once thawed, the cells were quickly transferred to a laminar flow hood, then into a cell culture flask (CM-R126, procell), labeled, and placed in an incubator. The following day, the medium was replaced based on the condition of the cells. When cell density reached 80–90%, passage of the cells was necessary. Remove the cell culture supernatant and wash the cells twice with 1 × PBS. Add 0.25% trypsin (containing 0.02% EDTA) to digest the cells. Once the cells round up, halt the digestion by adding medium, then transfer the cell suspension into a 10 ml centrifuge tube. centrifuge at 1000 rpm for 3 min, discard the supernatant, and resuspend the cells in fresh medium. Divide the cell suspension at a 1:3 ratio into labeled Petri dishes and incubate. In accordance with experimental requirements, cells were seeded in 6-well plates and 6 cm dishes. Similar to the cell

passage procedure, the cells were diluted as necessitated by the experiment. Approximately 2 × 105 cells per well for the 6-well plates were evenly distributed onto the culture plates, labeled, and then incubated. The experiment proceeded once the cells had fully adhered.

Primary rat DRG cells (CP-R126, Procell) were cultured in procell rat DRG cell complete medium (CM-R126, Procell) at 37 ℃ with 5% CO_2. Cells were verified using immunofluorescence neurofilament light chain (NEFL) staining.

To explore the role of TMEM16A in rapamycin-induced autophagy, cells were transfected with TMEM16A interference and overexpression vectors, or an empty vector. Preparation for transfection began when cell density reached 70% (considering the volume of medium in a 6 cm dish is double that in a 6-well plate). The cells' culture medium was replaced with 1 ml of serum-free medium. In two sterile EP tubes, 125 ul of Opti-MEM was added to each, with 5 ul of Lipofectamine 3000 to one tube and 12.5 ul of siRNA (siRNA dry powder reconstituted in DEPC water; 125 ul/1od) or overexpression vector + 10 ul/ug DNA p3000 to the other tube; both were mixed well and incubate at room temperature for 5 min. The contents of the two tubes were then combined and incubated at room temperature for 15 min before the mixture was added dropwise to the corresponding well in the 6-well plate, and cells were returned to the incubator. After 4–6 h of transfection, 1 ml of complete medium containing 20% serum was added to each well. Follow-up experiments proceeded 48 h post-transfection. At this point, the cells were categorized into five groups: control, nc+rap, si-tmem16a+rap, tmem16a+oe+rap and rap+sb203580. The cells were treated with 50 nm rap (hy-10219, nmce) for 24 h. The Rap+sb203580 group also received 15 μ M SB203580 treatment for the same period. Following evaluation by the medical ethics committee of Shenzhen Hospital (Futian), Guangzhou University of traditional Chinese medicine, this study, being an in vitro experiment that involves neither humans nor animals, does not necessitate ethical approval.

Identification of Primary Rat DRG Cells

The cells were cultured until optimal conditions were achieved, then the supernatant was discarded, and the cells were washed thrice with PBS. They were fixed with 4% paraformaldehyde at room temperature for 15 min, blocked with 5% BSA at 37 °C for 30 min, and then incubated overnight at 4 °C with β- Tubulin antibody (AF7011, Affinity, 1/200). The following day, Alexa fluor 488 labeled fluorescent secondary antibody (SA00006-2, proteintech, 1/200) was added and incubated at 37 °C for 30 min. After counterstaining with DAPI, the cells were observed under a fluorescence microscope (DS-Ri2, Nikon).

CCK8 Detection

Cells from each group were harvested, and 10 μL of CCK8 reagent (KGA317, Kaiji biological) was added. They were then incubate at 37 ℃ for 2 h before the absorbance at 450 nm was measured using a microplate reader (WD-2012B, Beijing 61).

Annexin V/Propidium Iodide Assay

Collect between 1 × 106 and 3 × 106 cells, add 1 ml of PBS, and centrifuge at 1500 rpm for 3 min, then wash twice. Dilute 5 × Binding Buffer to 1 × Binding Buffer using double distilled water. Resuspend the cells in 300 ul of precooled 1 × Binding Buffer. To each tube, add 5 ul of Annexin V-FITC and 10 ul of PI. Gently mix and incubate at room temperature in the dark for 10 min. Add 200 ul of precooled 1 × Binding Buffer to each tube. After mixing, proceed to detection using a flow cytometer.

Transmission Electron Microscopy (TEM) Examination

Fix DRG cells using 2.5% glutaraldehyde and wash with PBS buffer three times, for 10 min each. Prepare for fixation in phosphate buffer for a minimum of 2 h (rinse three times with 0.1 M phosphate buffer for 15 min; fix 2–3 h with 1% osmium tetroxide; rinse again three times with 0.1 M phosphate buffer for 15 min). Dehydrate the samples in a 4 ℃ refrigerator, following a stepwise process (15–20 min in 50% ethanol; 15–20 min in 70% ethanol; 15–20 min in 90% ethanol; 15–20 min in a 1:1 mixture of 90% ethanol and 90% acetone; 15–20 min in 90% acetone); Then further dehydrate with 100% acetone at room temperature, repeating this step three times for 15–20 min each. After fixing the cells, replace the alcohol with 100% acetone for 10 min before proceeding with the infiltration of Spurr's epoxy resin at room temperature, following a gradual concentration increase (acetone: Spurr's epoxy resin = 3:1 for 2 h; 1:1 for 3 h; 1:3 overnight. Then, pure Spurr's epoxy resin for 36 h). Enhance infiltration by shaking and rotating on a rotary mixer. Embed and polymerize at 70 ℃ for 48 h, then continue embedding at room temperature (pure acetone: embedding solution = 2:1 for 3–4 h; 1:2 overnight; pure embedding solution at 37 ℃ for 2–3 h). After embedding, cure the samples (overnight at 37 °C; 12 h at 45 °C; 48 h at 60 °C). Subsequently, cut sections with a thickness of 70–90 nm using an ultra-microtome (Leica UC 7) and double stain with 10.3% uranyl acetate and lead citrate.

Finally, the cells were observed and images were captured using a fluorescence microscope (ds-ri2, Nikon). 9 images were taken and have been added to the supplementary file. (DAPI UV excitation wavelength 330–380 nm, emission

wavelength 420 nm, producing blue light; FITC excitation wavelength 465–495 nm, emission wavelength 515–555 nm, generating green light; Cy3 excitation wavelength 510–560, emission wavelength 590 nm, producing red light. Nuclei stained with DAPI appear blue under UV light, and positive expression is indicated by the fluorescein-labeled green light).

Real-Time Fluorescence Quantitative PCR (qPCR)

qPCR was employed to measure the expression levels of p38 MAPK, mTOR, Beclin-1, ATG5, LC3A. LC3B, and P62 in the cells. Total RNA in cells was extracted using Trizol reagent (CW0580S, CWBIO), and further purification was performed with the RNA UltraPure Extraction Kit (CW0581M, CWBIO). The concentration and purity of the RNA (OD260/OD280 ratio) were assessed using a UV–VIS spectrophotometer. cDNA was synthesized using RNA reverse transcription kit, and qPCR was conducted using fluorescence PCR instrument (CFX Connect, Bio-Rad). The reaction protocol included: initial denaturation at 95 °C for 10 min; denaturation at 95 °C for 10 s; annealing at 58 °C for 30 s; extension at 72 °C for 30 s, over 40 cycles. GAPDH served as the internal control. The relative gene expression was calculated using the $2^{-\Delta\Delta Ct}$ method. Primer sequences are provided in the table below (Table 1).

Western Blot

The cells were harvested and the culture medium discarded. Total protein was extracted using RIPA lysis buffer (C1053, Applygen) and then centrifuged at 4 ℃ for 10 min at 12,000 rpm using a high-speed centrifuge (5424R, Eppendorf). The supernatant was collected, and protein concentration quantified using BCA Protein Quantification Kit (E-BC-K318-M, Elabscience). Protein samples were denatured and subjected to sodium dodecyl sulfate–polyacrylamide gel electrophoresis (SDS-PAGE) for 1.5 h, followed by transfer onto a PVDF membrane (Millipore) at a constant current of 300 mA for 1 h. The membrane was blocked with skim milk powder, incubated with the primary antibody overnight at 4 °C, and then with the secondary antibody at room temperature for 2 h the following day. The membrane was treated with hypersensitive luminescent solution (RJ239676, Thermo Fisher) and developed using an ultra-high sensitivity chemiluminescence imaging system (Tanon-5200, Shanghai Tianneng Technology Co., Ltd.). The antibodies used and their respective dilutions are listed in the table below. The specificity of all primary antibodies used has been authenticated through knockout by the initial manufacturer. (Information about the knockout validation of the primary antibodies are found in Appendix 2 of the supplement. Standardized data is the ratio of the relative molecular weight of relevant proteins to the relative molecular weight of β—actin) (Table 2).

Statistic Analysis

Graphs and statistical analyses were performed using GraphPad Prism 9.0 and SPSS 22.0. Quantitative data are presented as the mean ± standard deviation (X ± SD). Initially, the Shapiro–Wilk test and Levene's test were applied to assess the normality and homogeneity of variance, respectively. For data adhering to normal distribution, comparisons between two groups were made using an independent sample t-test, while one-way ANOVA was utilized for multiple group comparisons. For non-normally distributed data, the Mann–Whitney U test, the Kruskal–Wallis tests followed by Tukey's post hoc test was employed. A p-value < 0.05 was deemed statistically significant. The sample size for the experimental design ($n = 10$) was established based on prior experimental research in the same domain and acceptable SD values (Zhang et al. 2018b). This study acknowledges certain limitations, including the omission of an initial sample size calculation. (The results of the tests for normality and variance homogeneity are found in Appendix 3 of the supplement).

Table 1 Primer sequences

Primers	Forward primer F (5′-3′)	Reverse primerR (5′-3′)
TMEM16A	CTCTTCGCCCTGCTGAACAA	TGAGAATGTTATACCAGATGCCG
Beclin-1	GGAGAAAGGCAAGATTGAAGA	AGGACACCCAAGCAAGACC
ATG5	GAACGAGAAGCAGAGCCATACT	GGTCCAAAACTGGTCAAATCAT
LC3A	TTCGCCGACCGCTGTAA	ATCCGTCTTCATCCTTCTCCTG
LC3B	ATAGAGCGATACAAGGGTGAGAAG	CAGGAGGAAGAAGGCTTGGTTAG
P62	CCAGAGTCAAGGGGAGTCAG	GGGTGCTCTCTGTATGCTCC
p38MAPK	ACACTCGGCTGACATAATCCA	CACGGACCAAATATCCACTGTCT
mTOR	GAAGGTCACTGAGGATTTGTCCA	AGTGTATCCTGGAGGTTGTTG
GAPDH	GACAACTTTGGCATCGTGGA	ATGCAGGGATGATGTTCTGG

Table 2 List of antibodies

Antibody name (product number, manufacturer)	RRIDs	Dilution multiple
Mouse Anti-β-actin (TransGen Biotech)	HC_201	1:2000
HRP labeled IgG (H + L) (Servicebio)	GB23301/GB23303	1:2000
Rabbit Anti Atg5(Abcam)	AB_108327	1:1000
Rabbit Anti P62 (Proteintech)	66184-1-Ig	1:10000
Rabbit Anti mTOR (Proteintech)	66888-1-Ig	1:5000
Mouse Anti p38 (Thermo)	MA5-15116	1:1000
Rabbit Anti p-p38/MAPK (Thr180/Tyr182) (Proteintech)	28796-1-AP	1:2000
Rabbit Anti TMEM16A (Affinity)	DF_7769	1:1000
Rabbit Anti LC3 (abcam)	AB_192890	1:1000
Rabbit Anti Beclin-1 (Proteintech)	11306-1-AP	1:4000

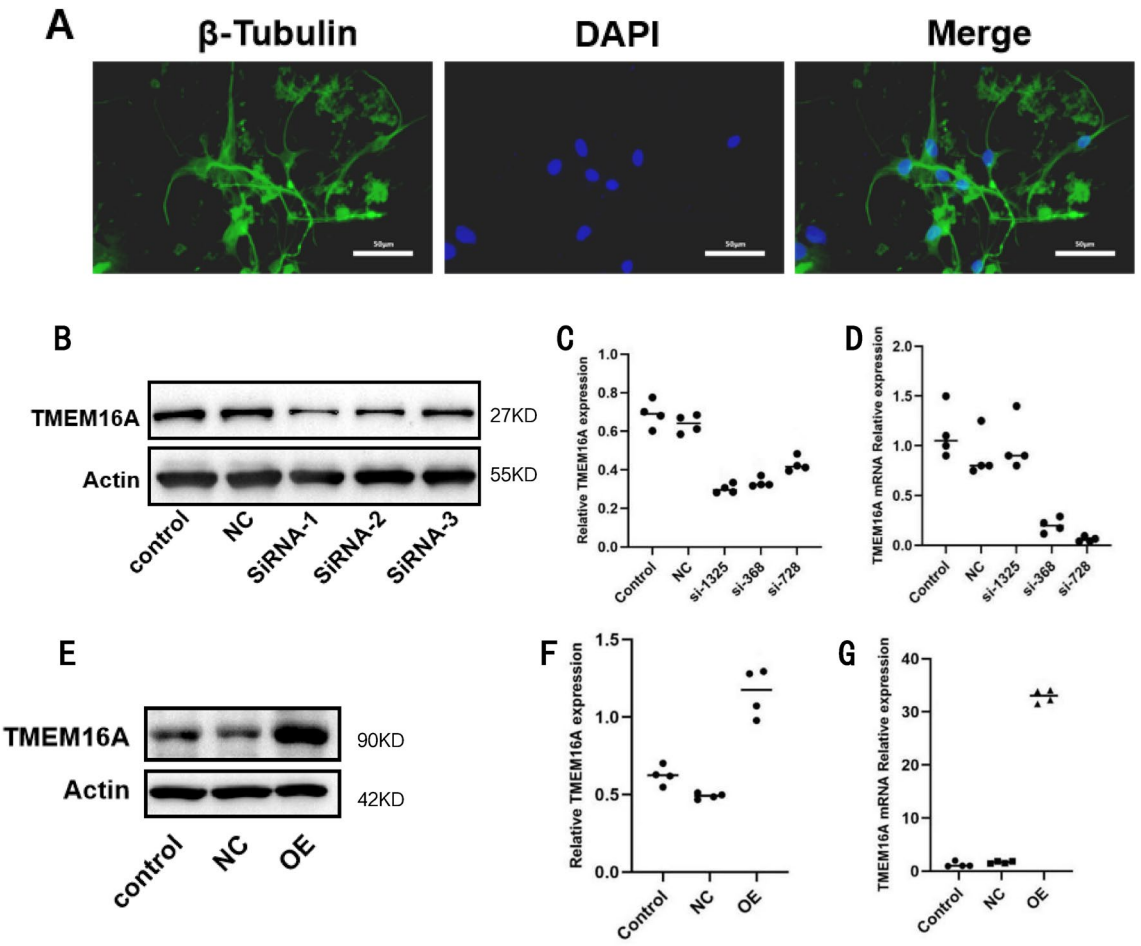

Fig. 1 (**A**) Elevated β-Tubulin expression observed in these cells; (**B**–**D**) WB and QPCR analyses verify interference efficiency (n = 4); (**E**–**G**) WB and QPCR analyses confirm overexpression efficiency (n = 4) (*P < 0.05 compared to the NC group)

Result

Validation of TMEM16A Overexpression and Interference Proves Effective

To elucidate TMEM16A's role in Rap-induced autophagy, cells were transfected with TMEM16A interference and overexpression vectors, or an empty vector. Immunofluorescence was employed to detect β-Tubulin in primary rat DRG cells, revealing robust β-Tubulin expression indicative of neuronal axonal and dendritic structures (Fig. 1A). The observed axonal and dendritic structures are typical of neurons. The efficacy of transfection with TMEM16A interference vectors (three designed, one selected) and an

overexpression vector was validated using QPCR and Western Blot (WB), demonstrating that all three interferences were effective (Fig. 1B). Interference 1 was identified as the most effective and selected for further experiments. Furthermore, the overexpression vector markedly increased TMEM16A expression (Fig. 1C). The data description is as follows (Tables 3, 4).

TMEM16A Inhibits Cell Viability and Rap-Induced Apoptosis

To assess the impact of TMEM16A on cell viability and Rap-induced apoptosis, cell viability was evaluated using CCK8, and apoptosis was measured by flow cytometry across all groups. The cell viability and apoptosis data were normally distributed, but showed heterogeneity in variance, prompting the use of non-parametric rank sum tests for statistical analysis. The findings revealed that Rap treatment significantly reduced cell viability (Mann–Whitney $U = 828.8$, $P < 0.0001$). Conversely, TMEM16A interference promoted cell viability ($P < 0.0001$), whereas its overexpression inhibited cell viability ($P = 0.0134 < 0.05$). Additionally, co-treating cells with Rap and SB203580 counteracted the rapamycin-induced reduction in DRG cell viability ($P < 0.0001$; Fig. 2A).

Flow cytometry showed that Rap treatment increased cell apoptosis (Mann–Whitney $U = 93.43$, $P < 0.0001$). However, TMEM16A interference did not reduce Rap-induced apoptosis ($P = 0.672 > 0.05$), while overexpression of TMEM16A decreased the apoptosis rate ($P = 0.04 < 0.05$). Moreover, SB203580 significantly lowered the apoptosis rate ($P < 0.0001$). These results indicate that TMEM16A interference boosts cell viability but does not counteract apoptosis triggered by Rap. On the other hand, overexpression of TMEM16A does not promote cell viability but can inhibit Rap-induced apoptosis (Fig. 2B).

Table 4 The relative expression data of TMEM16A overexpression vectors

TMEM16A relative expression	Control	NC	OE
mRNA	0.965670571	1.856083793	31.5224067
	1.029959912	1.852703817	34.04832238
	1.00542732	1.464304396	32.21986313
	1.986083793	1.522406699	33.85270382
Protein	0.702377441	0.498092294	0.978727034
	0.548579564	0.46737224	1.279106858
	0.619207764	0.512221994	1.294082327
	0.628727034	0.485579564	1.072377441

TMEM16A Enhances p38 MAPK/mTOR mRNA and Protein Expression

To examine TMEM16A's effect on the p38 MAPK/mTOR pathway, QPCR analysis and Western blotting were employed to determine the gene and protein expression levels of TMEM16A, p38 MAPK, and mTOR in each cell group. The expression data for TMEM16A, p38 MAPK, and mTOR genes and proteins exhibited a normal distribution. Variance for TMEM16A data was uneven, while variance for p38 MAPK and mTOR data was homogeneous. Accordingly, non-parametric rank sum tests were applied to the TMEM16A data, and One Way ANOVA followed by Tukey's post hoc tests were used for the p38 MAPK and mTOR genes and proteins analysis.

The findings revealed that the gene expression levels of TMEM16A, p38 MAPK, and mTOR were significantly elevated following Rap stimulation (Mann–Whitney $U = 2944$, $F = 1779, 108.4$; $P = 0.0361 < 0.05$, $P < 0.0001$, $P < 0.0001$). Interference with TMEM16A reduced the Rap-induced increase in p38 MAPK and mTOR gene expression ($P < 0.0001$, $P < 0.0001$), while overexpression of TMEM16A enhanced their expression levels ($P = 0.02 < 0.05$, $P < 0.0001$). SB203580 counteracted the Rap-induced upregulation of TMEM16A and decreased p38 MAPK and

Table 3 The relative expression data of TMEM16A interference vectors

TMEM16A relative expression	Control	NC	Si-1325	Si-368	Si-728
mRNA	1.1	0.8	0.8	0.115	0.03985
	1.5	1.25	1.4	0.224	0.06534
	1	0.75	0.9	0.289	0.09432
	0.9	0.8	0.9	0.172	0.04049
Protein	0.700893514	0.684682441	0.282122098	0.32259579	0.482910713
	0.602037923	0.584944719	0.284540325	0.37069249	0.394235156
	0.775563463	0.67071377	0.333615039	0.316964106	0.420874971
	0.68071377	0.612037923	0.306964106	0.323615039	0.412037923

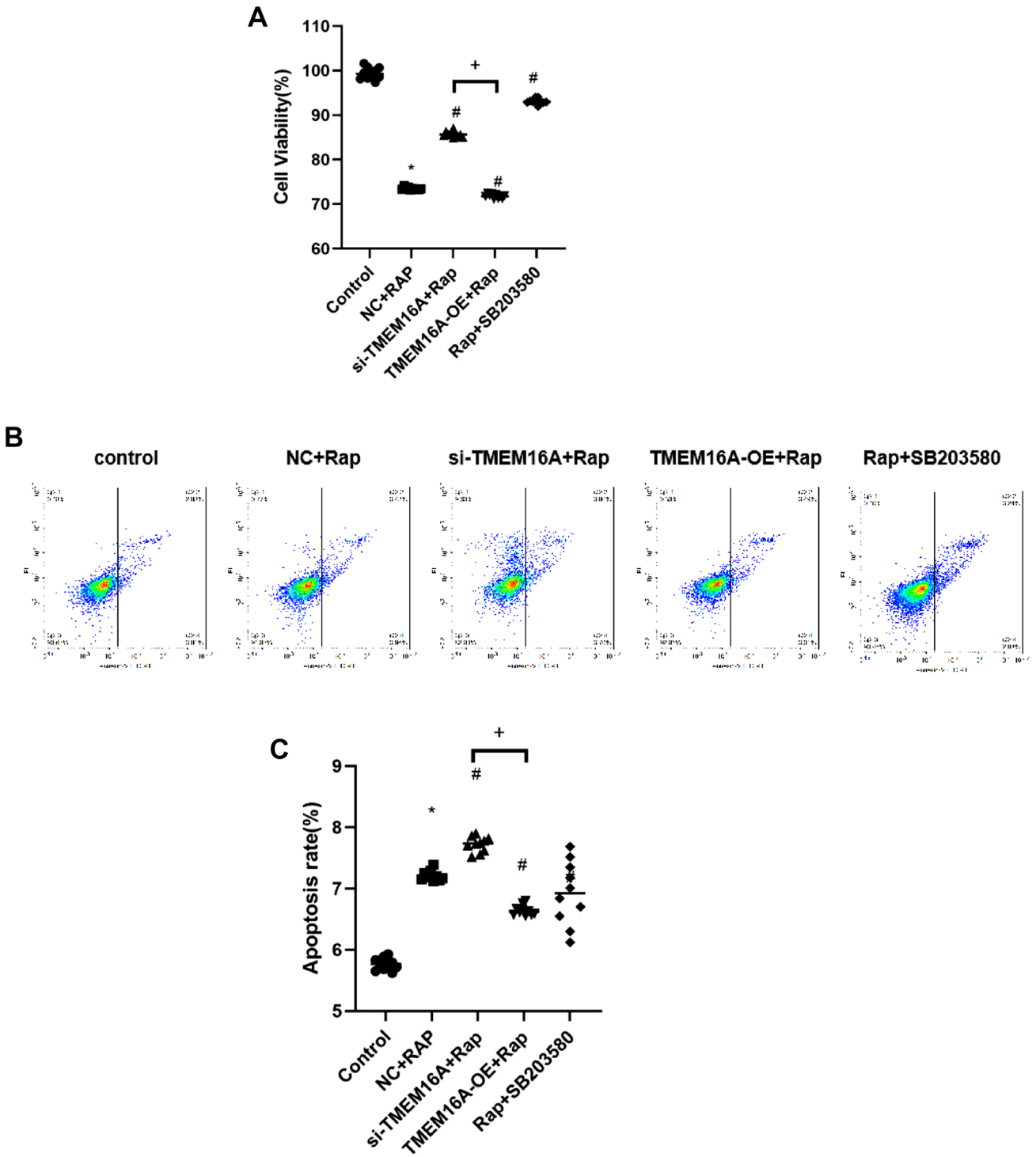

Fig. 2 Following transfection with the relevant vectors for 48 h, dorsal root ganglion cells were subjected to treatment with Rap, or a combination of Rap and SB203580 for 24 h. (**A**) TMEM16A reduces cell viability (n = 10); (**B**, **C**) TMEM16A facilitates apoptosis (n = 10). * Compared with Control, $P < 0.05$; # Compared with NC + Rap, $P < 0.05$; +Si-TMEM16A+Rap compared with TMEM16A+oe+Rap, $P < 0.05$

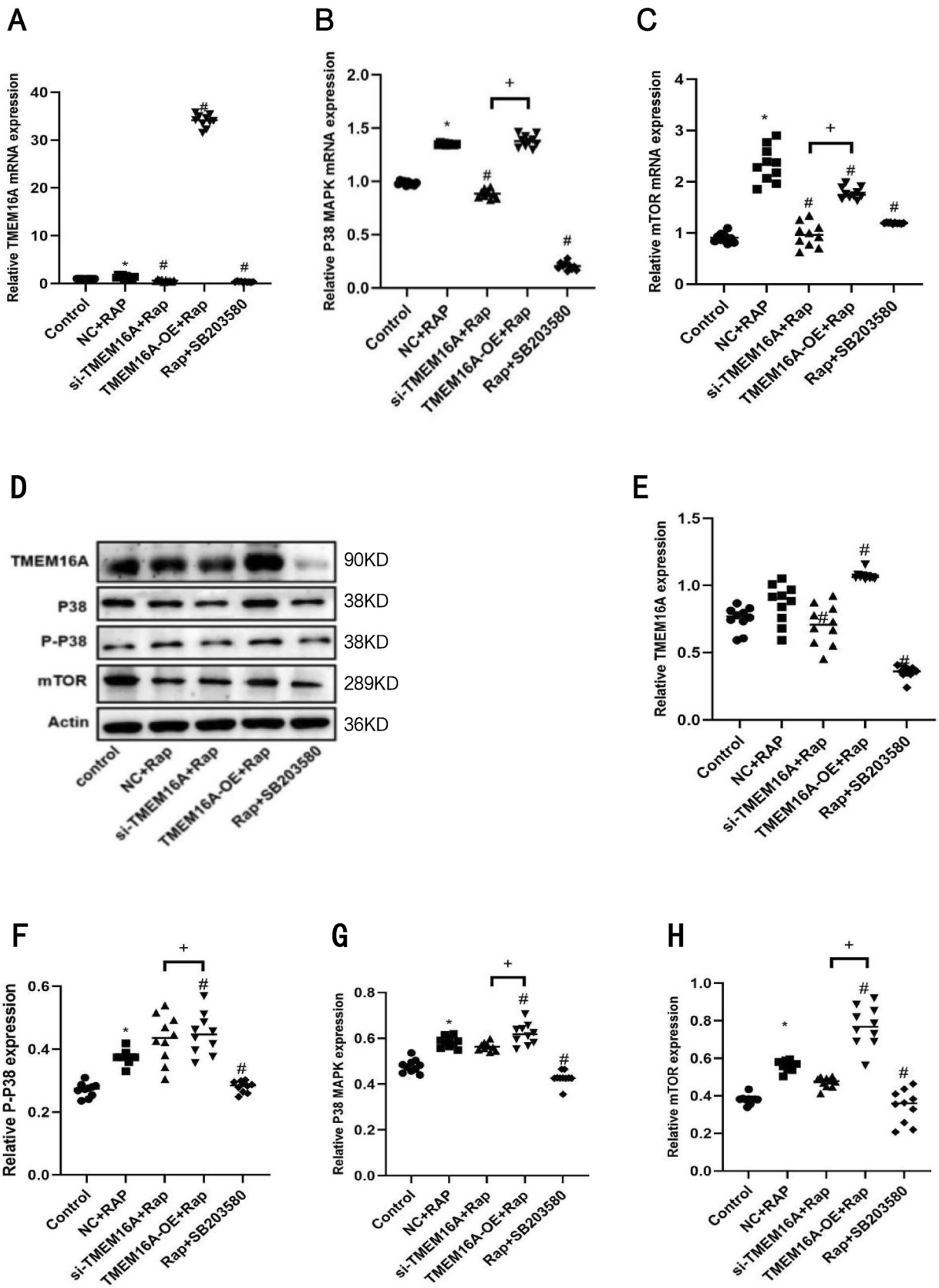
A
Relative TMEM16A mRNA expression
40
30
20
10
0
Control
NC+RAP
si-TMEM16A+Rap
TMEM16A-OE+Rap
Rap+SB203580
B
Relative P38 MAPK mRNA expression
2.0
1.5
1.0
0.5
0.0
C
Relative mTOR mRNA expression
4
3
2
1
0
D
TMEM16A
P38
P-P38
mTOR
Actin
90KD
38KD
38KD
289KD
36KD
control
NC+Rap
si-TMEM16A+Rap
TMEM16A-OE+Rap
Rap+SB203580
E
Relative TMEM16A expression
1.5
1.0
0.5
0.0
F
Relative P-P38 expression
0.6
0.4
0.2
0.0
G
Relative P38 MAPK expression
0.8
0.6
0.4
0.2
0.0
H
Relative mTOR expression
1.0
0.8
0.6
0.4
0.2
0.0

◂**Fig. 3** (**A**–**C**) TMEM16A increases mRNA expression of p38 MAPK and mTOR (n = 10); (**D**–**H**) TMEM16A enhances protein expression of p38 MAPK and mTOR (n = 10). * Compared with control, $P < 0.05$; # Compared with NC+Rap, $P < 0.05$; +si-TMEM16A + Rap compared with TMEM16A+oe+Rap, $P < 0.05$

mTOR gene expression (P < 0. 0001). Furthermore, gene expression of p38 MAPK and mTOR was notably higher in the overexpression group compared to the interference group (P < 0. 0001, Fig. 3A).

Results of Western blotting analysis indicated that Rap treatment significantly enhanced p38 phosphorylation and mTOR protein expression (F = 36.79, 33.4; P = 0.01 and P = 0.005, respectively, both below 0.05). The overexpression group exhibited further elevations in p38 phosphorylation and mTOR protein levels (P = 0.0128 and P = 0.0212, respectively, both below 0.05). Conversely, SB203580 suppressed TMEM16A expression, p38 phosphorylation, and mTOR levels (P < 0. 0001). Furthermore, p38 phosphorylation and mTOR protein expression levels were markedly elevated in the overexpression group as compared to the interference group (P = 0.0130 and P < 0.0001, respectively; Fig. 3B).

TMEM16A Facilitates Autophagy in DRG Cells

To further investigate TMEM16A's impact on autophagy, we observed autophagosome formation in DRG cells using TEM and QPCR analysis. Additionally, Western blotting was employed to assess the expression levels of genes and proteins associated with autophagy, including P62, Beclin-1, LC3A, LC3B, and ATG5, in each cell group. The distribution of autophagy-related gene and protein data was found to be normal. However, the variance in P62 data was heterogeneous, while the variance for Beclin-1, LC3A, LC3B, and ATG5 was homogeneous. Consequently, we employed non parametric rank sum tests to analyze the P62 data, and One Way ANOVA with post hoc tests for the the gene and protein data of Beclin-1, LC3A, LC3B, and ATG5.

The TEM findings revealed no autophagosomes were observed in the control group. In contrast, the NC+Rap group exhibited 4 autophagosomes, si−TMEM16A+Rap group displayed 8 autophagosomes, TMEM16A+OE+Rap group showed 2 autophagosomes, and Rap+SB203580 group presented 5 autophagosomes. In short, an increase in autophagosomes following Rap treatment, which was further enhanced with TMEM16A interference and significantly decreased following TMEM16A overexpression. Autophagy levels rose following co-treatment with SB203580 (Fig. 4A).

The qPCR results demonstrated that the gene expression levels of P62, LC3A, LC3B, and ATG5 were significantly elevated under Rap stimulation (Mann–Whitney U = 345. 6; F = 56. 69, 41. 47, 56. 04; P = 0.0182, P < 0.0001, P = 0.04, P < 0.0001, respectively, all below 0.05). TMEM16A interference further increased the expression of P62, Beclin-1, and LC3B (P < 0. 0001, P < 0. 0001, P = 0.0488, respectively, all below 0.05), while its overexpression also elevated P62 and LC3B expression (P < 0.0001 and P = 0.02, respectively, both below 0.05), but suppressed LC3A expression (P < 0. 0001). SB203580 boosted the expression of P62, Beclin-1, and LC3B (P = 0.0026, P < 0.0001, P = 0.0049, respectively, all below 0.05). Moreover, compared with TMEM16A+oe+Rap, the gene expression levels of P62, Beclin-1, and LC3A were significantly higher in si-TMEM16A+Rap (P < 0.0001 for each), whereas LC3B and ATG5 exhibited no significant difference (P = 0.0657 and P = 0.7944, respectively, both above 0.05; Fig. 4B).

Results of Western blotting revealed that Rap treatment significantly increased the protein expression of P62 and LC3B (Mann–Whitney U = 49. 61, F = 17. 14; P < 0.0001 and P = 0.0335, respectively, both below 0.05), while it reduced the expression of LC3A and ATG5 (F = 19.93 and 43,041; P = 0.0414 and P < 0.0001, respectively). TMEM16A interference further elevated the expression of P62 and ATG5 (P = 0.0032 and P < 0.0001, respectively, both below 0.05). TMEM16A overexpression additionally enhanced the level of Beclin-1, LC3A, LC3B and ATG5 (P = 0.0056, P = 0.0014, P = 0.0011, and P = 0.0362, respectively, all below 0.05). SB203580 also increased the levels of P62, Beclin-1 and ATG5 (P = 0.0047, P = 0.0061, and P = 0.0051, respectively, all below 0.05). Additionally, the protein expression levels of P62, LC3A, LC3B and ATG5 were significantly elevated in si-TMEM16A+Rap compared with TMEM16A+oe+Rap (P < 0.0001, P = 0.006, P < 0.0001, and P < 0.0001, respectively), with no significant difference in Beclin-1 expression (P = 0.1463, above 0.05; Fig. 4C). (Full western blots showing the marker are found in Appendix 4 of the supplement).

Discussion

This study demonstrated that: (1) TMEM16A interference promotes cell viability, and its overexpression inhibits Rap-induced apoptosis; (2) TMEM16A, p38MAPK, and mTOR play a role in suppressing Rap-induced autophagy in DRG neurons; (3) TMEM16A is associated with p38MAPK/mTOR signaling pathway. In summary, TMEM16A activation inhibits autophagy in DRG cells, which is associated with the p38 MAPK/mTOR pathway.

In 2008, researchers identified TMEM16A as the molecular basis of CaCCs (Schroeder et al. 2008). It is a heat-sensitive protein known to contribute to various physiological and pathological functions, including NP (Chen et al. 2021a; Zhang et al. 2018a). Qin-Yi Chen et al. (Chen et al. 2019) reported an upregulation of TMEM16A protein expression

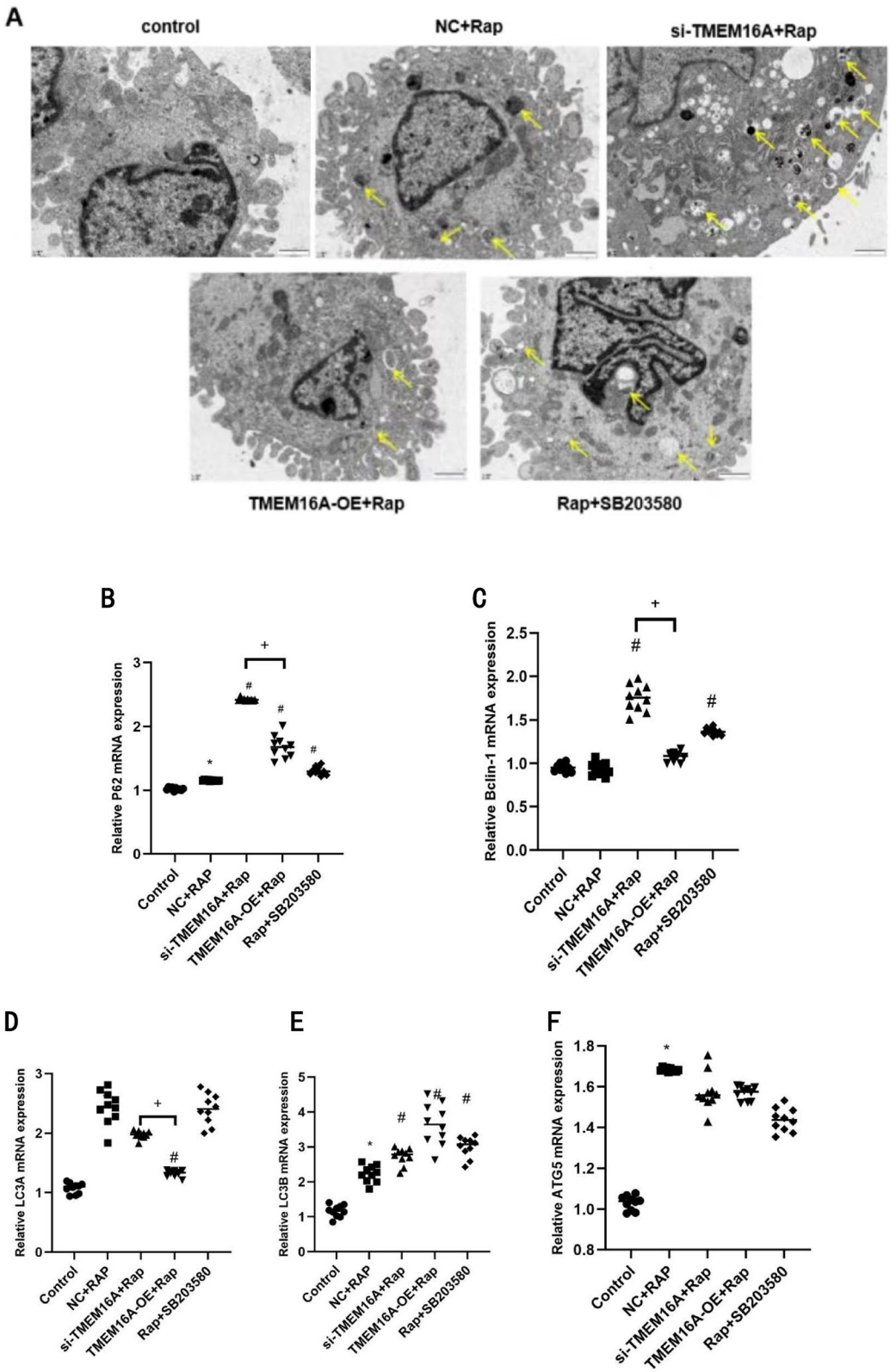

Fig. 4 (**A**) TEM showing TMEM16A inhibits the formation of autophagosomes. The yellow arrows indicated the autophagosomes of DRG cells. Scale bar = 4 μm for Control, NC+Rap, si−TMEM16A+Rap, and Rap+SB203580 groups, Scale bar = 1 μm for TMEM16A+OE+Rap group; (**B**–**F**) TMEM16A promotes mRNA expression of autophagy markers (P62, Beclin-1, LC3A, LC3B, and ATG5) in DRG neurons (n = 10); (**G**–**L**) TMEM16A elevates protein expression of autophagy markers (P62, Beclin-1, LC3A, LC3B, and ATG5) in DRG neurons (n = 10). * Compared with Control, $P < 0.05$; # Compared with NC+Rap, $P < 0.05$, +si-TMEM16A + Rap compared with TMEM16A+oe+Rap, $P < 0.05$

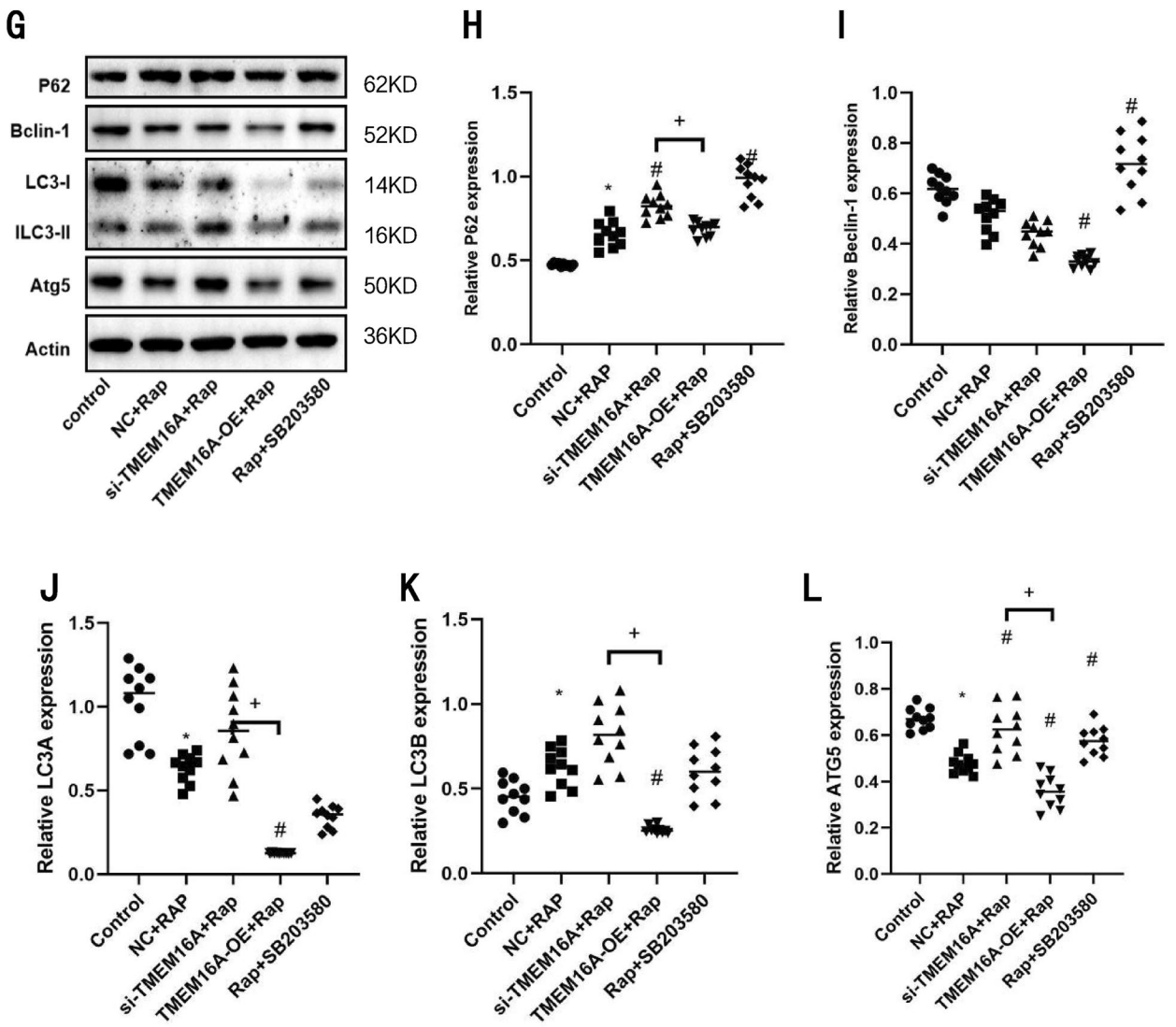

Fig. 4 (continued)

in DRG neurons of rats with a neuropathic pain model, indicating TMEM16A's role in sustaining NP. Previous research has established a negative correlation between NP and DRG autophagy, with autophagy alleviating NP and its progression (Li et al. 2021; Zhu et al. 2018; Xu et al. 2022). Thus, it is hypothesized that TMEM16A might suppress autophagy in DRG neurons, thereby sustaining NP.

DRG autophagy and apoptosis are often triggered by cellular damage or stress (Liao et al. 2022). Autophagy, a self-digestive process, entails protein and organelle degradation to enhance cell survival under stress (Wollert 2019). Initially, Beclin-1 of the endoplasmic reticulum responds to stress signals, initiating phagophore formation. Subsequently, various proteins, including autophagy-related protein 5 (ATG5), microtubule-associated protein 1A/1B light chain 3 (LC3), and P62, participate in autophagosome formation (Sun et al. 2009; Scervino et al. 2023; Han et al. 2022; He et al. 2018). Finally, autophagosomes merge with lysosomes, resulting in autolysosome formation and subsequent degradation (Lorincz and Juhasz 2020; Tian et al. 2021).

To investigate the relationship between TMEM16A and autophagy, we utilized Rap to induce autophagy in primary rat DRG cells and transfected them with TMEM16A interference, overexpression vectors, and an empty vector. TEM observations revealed a significant increase in autophagosomes following TMEM16A interference, corroborated by qPCR and Western blot results. This intervention resulted in elevated gene and protein expression levels of autophagy-related factors Beclin-1, P62, and LC3B. Numerous studies have indicated that the expression levels of LC3 B, bclin-1, and atg5-atg12 escalate with increased

autophagy activity (Bansal et al. 2018; Sun et al. 2009; Abulimiti et al. 2022; Wang et al. 2018b). Conversely, P62 expression, which facilitates the transport of ubiquitinated cargo to autophagosomes, decreases (Rusten and Stenmark 2010; Misra and Dikic 2019). Nonetheless, some researchers argue that a rise in LC3-B expression suggests blocked autophagic flux and diminished autophagic activity (Giménez-Xavier et al. 2008). Our qPCR and Western blot data showing increased P62 and LC3-B levels upon TMEM16A overexpression further support the notion that TMEM16A negatively regulates autophagy in DRG neurons. Apoptosis, a form of programmed cell death and cellular atrophy (Fig. 5) (Chen et al. 2022), is observed to increase in animal studies after DRG injury, both in the DRG (Dastgheib et al. 2023; Ozdemir et al. 2023; Shao et al. 2021; Dong et al. 2021) and the spinal cord (Zhou et al. 2016; Özdemir et al. 2016). Post-Rap induction, cell viability assays and flow cytometry revealed that TMEM16A interference promotes cell viability, while its overexpression inhibits Rap-induced apoptosis.

MAPK is a crucial cellular signal transduction pathway involved in regulating cell growth and differentiation (Lin et al. 2022). Recent findings suggest that p38MAPK, an intracellular signal transducer, plays a role in autophagy regulation (He et al. 2021; Lai et al. 2018) and acts as an upstream regulator of autophagy (Shen et al. 2021). MTOR, a serine or threonine protein kinase, is a key inhibitor of autophagy initiation (Wang et al. 2018a, 2018c). It phosphorylates ULK1, a vital autophagy protein, inhibiting its activity and thus autophagy (Wu et al. 2023; Chen et al. 2021b). Our TEM observations showed increased autophagosomes following p38MAPK inhibition. This also stimulated the gene expression of P62, Beclin-1, and LC3B, as well as the protein expression levels of ATG5, indicating that inhibiting p38MAPK significantly enhances autophagy activity.

The findings suggest that both TMEM16A and p38MAPK negatively regulate autophagy. However, the precise relationship between TMEM16A and p38MAPK/mTOR pathway remains unclear. To investigate this, we employed qPCR and Western blot analyses to measure the gene and protein

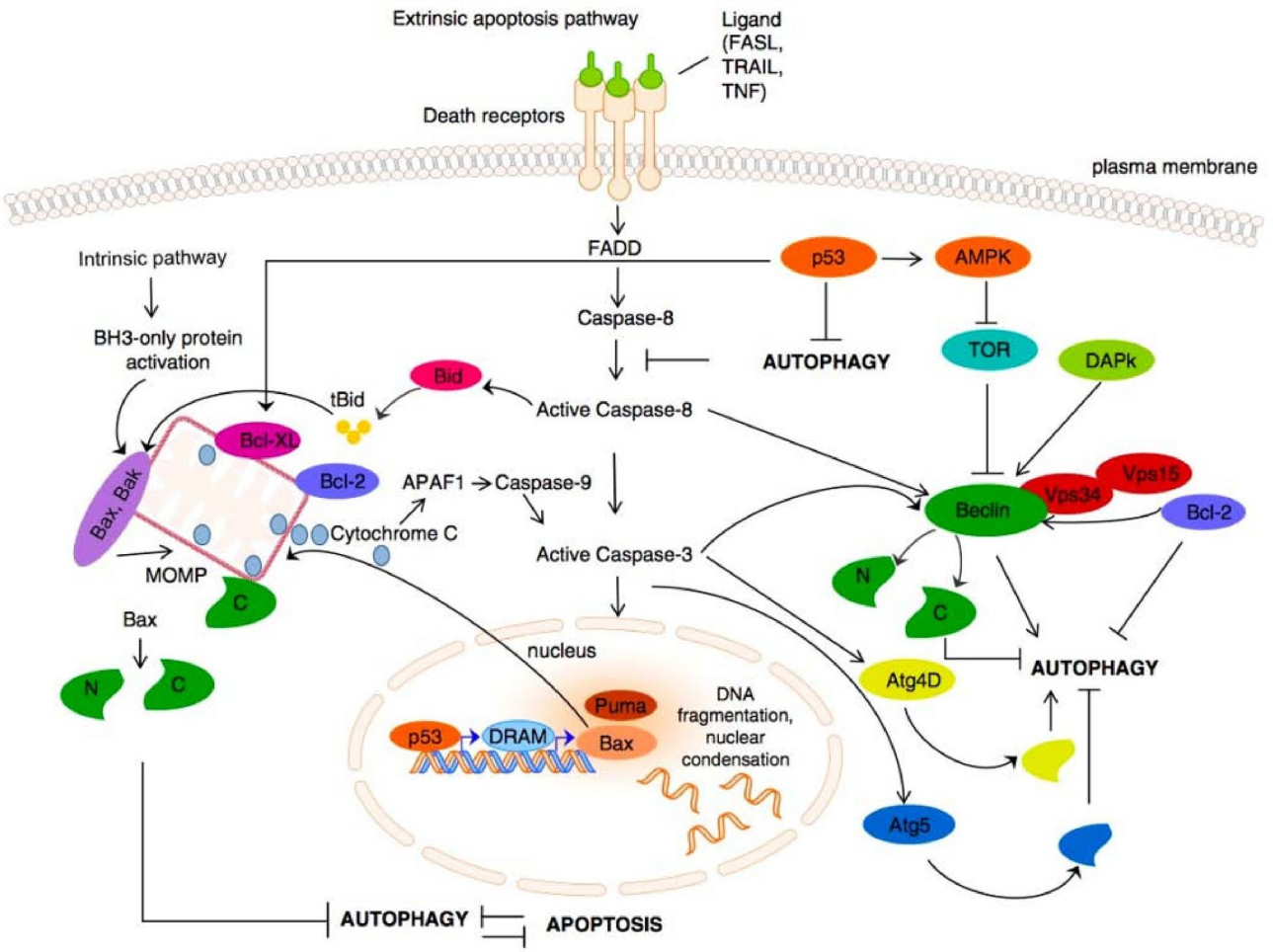

Fig. 5 Schematic diagram of signaling pathways involved in the interplay between autophagy and apoptosis (Nikoletopoulou et al. 2013)

expression levels of p38MAPK and mTOR following Rap-induced autophagy in DRG neuronal cells and subsequent TMEM16A interference or overexpression. The results demonstrated that TMEM16A overexpression led to increased gene and protein expression of p38MAPK and mTOR, whereas TMEM16A interference reduced their expression. This indicates that TMEM16A exerts a positive feedback effect on p38MAPK and mTOR.

In general, this study demonstrates that TMEM16A positively influences p38MAPK and mTOR. Specifically, it has been verified that TMEM16A activation inhibits autophagy in DRG cells, which is associated with the p38 MAPK/mTOR pathway.

Supplementary Information The online version contains supplementary material available at https://doi.org/10.1007/s10571-024-01507-z.

Author Contributions All authors contributed to the study conception and design. Y, S, J, Z, Y and Y performed research; S, QJ and analyzed data; The first draft of the manuscript was written by S, H, J and Y. All authors approved the final version of the manuscript.

Funding This work was supported by Futian Healthcare Research Project (NO.FTWS2023082), Shenzhen Science and Technology Program (NO.JCYJ202308073002360) and Shenzhen Science and Technology Program (NO.JCYJ20210324125608024).

Data Availability The datasets generated during and analysed during the current study are available in the figshare repository, https://doi.org/10.6084/m9.figshare.25033934.

Declarations

Competing interests The authors declare no competing interests.

References

Abulimiti G, Zeng JH, Aimaiti M, Lei XY, Mi N (2022) Harmol hydrochloride dihydrate induces autophagy in neuro cells and promotes the degradation of α-Syn by Atg5/Atg12-dependent pathway. Food Sci Nutr 10(12):4371–4379. https://doi.org/10.1002/fsn3.3031

Acharya B, Chaijaroenkul W, Na-Bangchang K (2021) Atractylodin inhibited the migration and induced autophagy in cholangiocarcinoma cells via PI3K/AKT/mTOR and p38MAPK signalling pathways. J Pharm Pharmacol 73(9):1191–1200. https://doi.org/10.1093/jpp/rgab036

Ali NH, Al-kuraishy HM, Al-Gareeb AI, Alnaaim SA, Alexiou A, Papadakis M, Saad HM, Batiha GE (2023) Autophagy and autophagy signaling in Epilepsy: possible role of autophagy activator. Mol Med 29(1):19. https://doi.org/10.1186/s10020-023-00742-2

Bansal M, Moharir SC, Swarup G (2018) Autophagy receptor optineurin promotes autophagosome formation by potentiating LC3-II production and phagophore maturation. Commun Integr Biol 11(2):1–4. https://doi.org/10.1080/19420889.2018.1467189

Bouhassira D, Lantéri-Minet M, Attal N, Laurent B, Touboul C (2008) Prevalence of chronic pain with neuropathic characteristics in the general population. Pain 136(3):380–387. https://doi.org/10.1016/j.pain.2007.08.013

Cai MY, Zhuang WX, Lv E, Liu Z, Wang YQ, Zhang WY, Fu WY (2022) Kaemperfol alleviates pyroptosis and microglia-mediated neuroinflammation in Parkinson's disease via inhibiting p38MAPK/NF-κB signaling pathway. Neurochem Int 152:16. https://doi.org/10.1016/j.neuint.2021.105221

Chen QY, Tan CY, Wang Y, Ma KT, Li L, Si JQ (2019) Mechanism of persistent hyperalgesia in neuropathic pain caused by chronic constriction injury. Neural Regen Res 14(6):1091–1098. https://doi.org/10.4103/1673-5374.250631

Chen QY, Kong LJY, Xu ZZ, Cao N, Tang XC, Gao RJ, Zhang JR, Deng SY, Tan CY, Zhang M, Wang Y, Zhang L, Ma KT, Li L, Si JQ (2021) The role of TMEM16A/ERK/NK-1 signaling in dorsal root ganglia neurons in the development of neuropathic pain induced by spared nerve injury (SNI). Mol Neurobiol 58(11):5772–5789. https://doi.org/10.1007/s12035-021-02520-9

Chen Z, Zhang JG, Dong CY, Li DS, Yin YH, Yu WH, Chen YZ (2021) TNFAIP8 regulates gastric cancer growth via mTOR-Akt-ULK1 pathway and autophagy signals. J Cell Mol Med 25(7):3361–3370. https://doi.org/10.1111/jcmm.16413

Chen FY, Ge Z, Li N, Yu ZC, Wu RB, Zhao Y, He XW, Cai GP (2022) TUDCA protects against tunicamycin-induced apoptosis of dorsal root ganglion neurons by suppressing activation of ER stress. Exp Ther Med 24(2):10. https://doi.org/10.3892/etm.2022.11436

Dastgheib M, Falak R, Moghaddam MV, Hassanzadeh G, Safa M, Hosseini A (2023) Rolipram and pentoxifylline combination ameliorates the morphological abnormalities of dorsal root ganglion neurons in experimental diabetic neuropathy by reducing mitochondrial dysfunction and apoptosis. J Biochem Mol Toxicol. https://doi.org/10.1002/jbt.23459

Debnath J, Leidal AM (2022) Secretory autophagy during lysosome inhibition (SALI). Autophagy 18(10):2498–2499. https://doi.org/10.1080/15548627.2022.2095788

Dong XQ, Zuo YF, Zhou M, Sun JJ, Xu PP, Chen B (2021) Bortezomib activation of mTORC1 pathway mediated by NOX2-drived reactive oxygen species results in apoptosis in primary dorsal root ganglion neurons. Exp Cell Res 400(2):9. https://doi.org/10.1016/j.yexcr.2021.112494

Estivill-Torrús G, Martínez-Padilla A, Sánchez-Salido L, Evercooren ABV, García-Díaz B (2024) The dorsal root ganglion as a target for neurorestoration in neuropathic pain. Neural Regen Res 19(2):296–301. https://doi.org/10.4103/1673-5374.374655

Giménez-Xavier P, Francisco R, Platini F, Pérez R, Ambrosio S (2008) LC3-I conversion to LC3-II does not necessarily result in complete autophagy. Int J Mol Med 22(6):781–785. https://doi.org/10.3892/ijmm_00000085

Gu Y, Ma LJ, Bai XX, Jie J, Zhang XF, Chen D, Li XP (2018) Mitogen-activated protein kinase phosphatase 1 protects PC12 cells from amyloid beta-induced neurotoxicity. Neural Regen Res 13(10):1842–1850. https://doi.org/10.4103/1673-5374.238621

Han NR, Moon PD, Nam SY, Ko SG, Park HJ, Kim HM, Jeong HJ (2022) TSLP up-regulates inflammatory responses through induction of autophagy in T cells. Faseb J 36(2):15. https://doi.org/10.1096/fj.202101447R

He JL, Dong XH, Li ZH, Wang XY, Fu ZA, Shen N (2018) Pterostilbene inhibits reactive oxygen species production and apoptosis in primary spinal cord neurons by activating autophagy via the mechanistic target of rapamycin signaling pathway. Mol Med Rep 17(3):4406–4414. https://doi.org/10.3892/mmr.2018.8412

He YX, Liu ZL, Huang YP, Li B (2021) Role of the p38MAPK signaling pathway in hippocampal neuron autophagy in rats with chronic intermittent hypoxia. J Neurophysiol 126(4):1112–1121. https://doi.org/10.1152/jn.00240.2021

Hou H, Yang YP, Chen R, Guo ZP (2023) Osthole protects H9c2 cardiomyocytes against trastuzumab-induced damage by enhancing autophagy through the p38MAPK/mTOR signaling pathway. Toxicol Vitro 93:10. https://doi.org/10.1016/j.tiv.2023.105704

Joo MC, Jang CH, Park JT, Choi SW, Ro S, Kim MS, Lee MY (2018) Effect of electrical stimulation on neural regeneration via the p38-RhoA and ERK1/2-Bcl-2 pathways in spinal cord-injured rats. Neural Regen Res 13(2):340–346. https://doi.org/10.4103/1673-5374.226404

Lai H-Y, Chen Q, Li H, Zhu C-H, Yi L-J, Zhou J, Hu Q-H, Yu X-J (2018) Role of p38MAPK signaling pathway in autophagy of Henle-407 cells induced by spvB of Salmonella typhimurium. Nan fang yi ke da xue xue bao = J Southern Med Univ 38(3):268–273

Li J, Tian ML, Hua T, Wang HW, Yang M, Li WQ, Zhang XP, Yuan HB (2021) Combination of autophagy and NFE2L2/NRF2 activation as a treatment approach for neuropathic pain. Autophagy 17(12):4062–4082. https://doi.org/10.1080/15548627.2021.1900498

Liao ZH, Zhang XH, Song CL, Lin WC, Cheng YZ, Xie Z, Chen S, Nie Y, Li AJ, Zhang HM, Li HX, Li HY, Xie QM (2020) ALV-J inhibits autophagy through the GADD45β/MEKK4/P38MAPK signaling pathway and mediates apoptosis following autophagy. Cell Death Dis 11(8):14. https://doi.org/10.1038/s41419-020-02841-y

Liao MF, Lu KT, Hsu JL, Lee CH, Cheng MY, Ro LS (2022) The role of autophagy and apoptosis in neuropathic pain formation. Int J Mol Sci 23(5):15. https://doi.org/10.3390/ijms23052685

Lin MX, Chen XH, Wu SY, Chen PZ, Wan HY, Ma SM, Lin N, Liao YL, Zheng T, Jiang JD, Zheng XC (2022) Upregulation of Na_v1.6 mediated by the p38 MAPK pathway in the dorsal root ganglia contributes to cancer-induced bone pain in rats. Cells 11(21):14. https://doi.org/10.3390/cells11213375

Lorincz P, Juhasz G (2020) Autophagosome-lysosome fusion. J Mol Biol 432(8):2462–2482. https://doi.org/10.1016/j.jmb.2019.10.028

Lv XF, Zhang YJ, Liu X, Zheng HQ, Liu CZ, Zeng XL, Li XY, Lin XC, Lin CX, Ma MM, Zhang FR, Shang JY, Zhou JG, Liang SJ, Guan YY (2020) TMEM16A ameliorates vascular remodeling by suppressing autophagy via inhibiting Bcl-2-p62 complex formation. Theranostics 10(9):3980–3993. https://doi.org/10.7150/thno.41028

Misra M, Dikic I (2019) RNA binding to p62 impacts selective autophagy. Cell Res 29(7):512–513. https://doi.org/10.1038/s41422-019-0167-2

Nikoletopoulou V, Markaki M, Palikaras K (2013) Tavernarakis N (2013) crosstalk between apoptosis, necrosis and autophagy. Biochim Biophys Acta-Mol Cell Res 1833 12:3448–3459. https://doi.org/10.1016/j.bbamcr.2013.06.001

Özdemir Ü, Naziroglu M, Senol N, Ghazizadeh V (2016) Hypericum perforatum attenuates spinal cord injury-induced oxidative stress and apoptosis in the dorsal root ganglion of rats: involvement of TRPM2 and TRPV1 channels. Mol Neurobiol 53(6):3540–3551. https://doi.org/10.1007/s12035-015-9292-1

Ozdemir E, Avci O, Inan ZDS, Taskiran AS, Gunes H, Gursoy S (2023) Aspirin attenuates morphine antinociceptive tolerance in rats with diabetic neuropathy by inhibiting apoptosis in the dorsal root ganglia. Metab Brain Dis 38(6):2145–2158. https://doi.org/10.1007/s11011-023-01226-2

Paul S, Dansithong W, Gandelman M, Figueroa KP, Zu T, Ranum LPW, Scoles DR, Pulst SM (2023) Staufen impairs autophagy in neurodegeneration. Ann Neurol 93(2):398–416. https://doi.org/10.1002/ana.26515

Qin XD, Yang TQ, Zeng JH, Cai HB, Qi SH, Jiang JJ, Cheng Y, Xu LS, Bu F (2023) Overexpression of mitogen-activated protein kinase phosphatase-1 in endothelial cells reduces blood-brain barrier injury in a mouse model of ischemic stroke. Neural Regen Res 18(8):1743–1749. https://doi.org/10.4103/1673-5374.363836

Ray SK (2020) Modulation of autophagy for neuroprotection and functional recovery in traumatic spinal cord injury. Neural Regen Res 15(9):1601–1612. https://doi.org/10.4103/1673-5374.276322

Rusten TE, Stenmark H (2010) p62, an autophagy hero or culprit? Nat Cell Biol 12(3):207–209. https://doi.org/10.1038/ncb0310-207

Scervino MVM, Fortes MAS, Vitzel KF, de Souza DR, Murata GM, Santana GO, da Silva EB, Levada-Pires AC, Kuwabara WMT, Loureiro TCA, Curi R (2023) Autophagy signaling in hypertrophied muscles of diabetic and control rats. FEBS Open Bio 13(9):1709–1722. https://doi.org/10.1002/2211-5463.13677

Schroeder BC, Cheng T, Jan YN, Jan LY (2008) Expression cloning of TMEM16A as a calcium-activated chloride channel subunit. Cell 134(6):1019–1029. https://doi.org/10.1016/j.cell.2008.09.003

Shao MH, Zheng CJ, Ma XS, Lyu FZ (2021) Ecto-5′-nucleotidase (CD73) inhibits dorsal root ganglion neuronal apoptosis by promoting the Ado/cAMP/PKA/CREB pathway. Exp Ther Med 22(6):9. https://doi.org/10.3892/etm.2021.10809

Shen YA, Zhang Y, Du JY, Jiang BC, Shan T, Li HJ, Bao HG, Si YN (2021) CXCR5 down-regulation alleviates cognitive dysfunction in a mouse model of sepsis-associated encephalopathy: potential role of microglial autophagy and the p38MAPK/NF-κB/STAT3 signaling pathway. J Neuroinflamm 18(1):16. https://doi.org/10.1186/s12974-021-02300-1

Sun QM, Fan WL, Zhong Q (2009) Regulation of Beclin 1 in autophagy. Autophagy 5(5):713–716. https://doi.org/10.4161/auto.5.5.8524

Tian XY, Teng JL, Chen JG (2021) New insights regarding SNARE proteins in autophagosome-lysosome fusion. Autophagy 17(10):2680–2688. https://doi.org/10.1080/15548627.2020.1823124

Torrance N, Smith BH, Bennett MI, Lee AJ (2006) The epidemiology of chronic pain of predominantly neuropathic origin. Results from a general population survey. J Pain 7(4):281–289. https://doi.org/10.1016/j.jpain.2005.11.008

Wang JF, Mei ZG, Fu Y, Yang SB, Zhang SZ, Huang WF, Xiong L, Zhou HJ, Tao W, Feng ZT (2018) Puerarin protects rat brain against ischemia/reperfusion injury by suppressing autophagy via the AMPK-mTOR-ULK1 signaling pathway. Neural Regen Res 13(6):989–998. https://doi.org/10.4103/1673-5374.233441

Wang N, Zhang QX, Luo LY, Ning BL, Fang YQ (2018) β-asarone inhibited cell growth and promoted autophagy via P53/Bcl-2/Bclin-1 and P53/AMPK/mTOR pathways in Human Glioma U251 cells. J Cell Physiol 233(3):2434–2443. https://doi.org/10.1002/jcp.26118

Wang SJ, Wang Q, Ma J, Yu PH, Wang ZM, Wang B (2018) Effect of moxibustion on mTOR-mediated autophagy in rotenone-induced Parkinson's disease model rats. Neural Regen Res 13(1):112–118. https://doi.org/10.4103/1673-5374.224380

Wollert T (2019) Autophagy. Curr Biol 29(14):R671–R677. https://doi.org/10.1016/j.cub.2019.06.014

Wu CC, Zeng LZ, Yi WF, Miao YJ, Liu YH, Wang QM, Liu S, Peng GP, Zheng ZH, Xia JB (2023) Echovirus induces autophagy to promote viral replication via regulating mTOR/ULK1 signaling pathway. Front Immunol 14:10. https://doi.org/10.3389/fimmu.2023.1162208

Xu Q, Niu C, Li JJ, Hu C, He ML, Qiu XZ, Yao Q, Tian WQ, Zhang MH (2022) Electroacupuncture alleviates neuropathic pain caused by spared nerve injury by promoting AMPK/mTOR-mediated autophagy in dorsal root ganglion macrophage. Ann Transl Med 10(24):15. https://doi.org/10.21037/atm-22-5920

Xu X, Chen R, Yu Y, Yang J, Lin C, Liu R (2023) Pulsed radiofrequency on DRG inhibits hippocampal neuroinflammation by regulating spinal GRK2/p38 expression and enhances spinal autophagy to reduce pain and depression in male rats with spared nerve injury. Int Immunopharmacol 127:111419. https://doi.org/10.1016/j.intimp.2023.111419

Yang LY, Wu YS, Lin SH, Dai BB, Chen H, Tao X, Li GP, Wan JX, Pan YB (2021) sPLA2-IB and PLA2R mediate insufficient autophagy and contribute to podocyte injury in idiopathic membranous nephropathy by activation of the p38MAPK/mTOR/ULK1^{ser757} signaling pathway. Faseb J 35(2):16. https://doi.org/10.1096/fj.202001143R

Zhang M, Gao CX, Wang YP, Ma KT, Li L, Yin JW, Dai ZG, Wang S, Si JQ (2018) The association between the expression of PAR2 and TMEM16A and neuropathic pain. Mol Med Rep 17(3):3744–3750. https://doi.org/10.3892/mmr.2017.8295

Zhang SS, Li JQ, Jiang HJ, Gao Y, Cheng PZ, Cao TQ, Li DL, Wang JM, Song Y, Liu B, Wu H, Wang CM, Yang L, Pei GX (2018) Dorsal root ganglion maintains stemness of bone marrow mesenchymal stem cells by enhancing autophagy through the AMPK/mTOR pathway in a coculture system. Stem Cells Int 2018:12. https://doi.org/10.1155/2018/8478953

Zhang D, Zhu D, Wang F, Zhu JC, Zhai X, Yuan Y, Li CX (2020) Therapeutic effect of regulating autophagy in spinal cord injury: a network meta-analysis of direct and indirect comparisons. Neural Regen Res 15(6):1120–1132. https://doi.org/10.4103/1673-5374.270419

Zhong J, Xuan WD, Tang MT, Cui SH, Zhou YH, Qu XS, Cao X, Niu B (2021) Advances in Anoctamin 1: a potential new drug target in medicinal chemistry. Curr Top Med Chem 21(13):1139–1155. https://doi.org/10.2174/1568026621666210607125614

Zhou J, Lin WJ, Chen HT, Fan YL, Yang CX (2016) TRESK contributes to pain threshold changes by mediating apoptosis via MAPK pathway in the spinal cord. Neuroscience 339:622–633. https://doi.org/10.1016/j.neuroscience.2016.10.039

Zhu Y-B, Jia G-L, Lu J-H, Zhang M-B, Li J, Cao H (2018) The relationship between autophagy activation in spinal cord and type 2 diabetic neuropathic pain in rats. Zhongguo ying yong sheng li xue za zhi = Zhongguo yingyong shenglixue zazhi = Chin J Appl Physiol 34(4):318–323. https://doi.org/10.12047/j.cjap.5644.2018.073

Authors and Affiliations

Shuyun Yang[1,2] · Hui Shang[1,2] · Yuruo Zhang[2] · Jingsong Qiu[3] · Zheyi Guo[1] · Yong Ma[1] · Yuhang Lan[1,2] · Shaoyang Cui[4] · Hongshuang Tong[1] · Guocai Li[1]

✉ Hongshuang Tong
623521637@qq.com

✉ Guocai Li
liguocai@gzucm.edu.cn

[1] Department of Anesthesiology, Shenzhen Hospital (Futian) of Guangzhou University of Chinese Medicine, Shenzhen 518034, Guangdong Province, China

[2] Sixth Clinical School of Medicine, Guangzhou University of Chinese Medicine, Shenzhen 518034, Guangdong Province, China

[3] The Fourth Clinical School of Guangzhou, University of Chinese Medicine, Shenzhen 518034, Guangdong Province, China

[4] Department of Rehabilitation, Shenzhen Hospital (Futian) of Guangzhou University of Chinese Medicine, Shenzhen 518034, Guangdong Province, China